NANO LETTERS

Letter

pubs.acs.org/NanoLett

Detection beyond the Debye Screening Length in a High-Frequency Nanoelectronic Biosensor

Girish S. Kulkarni and Zhaohui Zhong*

Department of Electrical Engineering and Computer Science, University of Michigan, Ann Arbor, Michigan 48109, United States

Supporting Information

ABSTRACT: Nanosensors based on the unique electronic properties of nanotubes and nanowires offer high sensitivity and have the potential to revolutionize the field of Point-of-Care (POC) medical diagnosis. The direct current (dc) detection of a wide array of organic and inorganic molecules has been demonstrated on these devices. However, sensing mechanism based on measuring changes in dc conductance fails at high background salt concentrations, where the sensitivity of the devices suffers from the ionic screening due to mobile ions present in the solution. Here, we successfully demonstrate that the fundamental ionic screening effect can be mitigated by operating single-walled carbon nanotube field effect transistor as a high-frequency biosensor. The nonlinear mixing between the alternating current excitation field and the molecular dipole field can generate mixing current sensitive to the surface-bound biomolecules. Electrical detection of monolayer streptavidin binding to biotin in 100 mM buffer solution is achieved at a frequency beyond 1 MHz. Theoretical modeling confirms improved sensitivity at high frequency through mitigation of the ionic screening effect. The results should promise a new biosensing platform for POC detection, where biosensors functioning directly in physiologically relevant condition are desired.

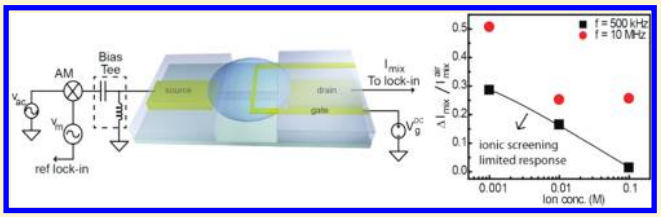

KEYWORDS: *Ionic screening, Debye length, carbon nanotube, high-frequency biosensor, frequency mixing*

Single-walled carbon nanotube (SWNT) and semiconductor nanowire (NW) based electronics[1−4] have been viewed as promising platforms for next generation chemical and biological sensors. Successful detection of a wide variety of molecules[5−11] has been demonstrated on these nanoelectronic platforms. The binding of charged molecules on such a sensor surface alters the carrier density in it through electrostatic gating and/or charge transfer,[12] resulting in changes in the direct current (dc) conductance of the sensor. The charge-detection based sensing mechanism has many advantages, including label-free detection,[13] femtomolar sensitivity[14] and electronic read out capability.[5] However, detecting charges in high ionic strength solutions is fundamentally impeded by ionic screening.[15−17] A charged surface in an ionic solution attracts counterions from the solution, forming an electrical double layer (EDL) and effectively screening off the charges. The columbic potential due to the surface falls off exponentially as we move away from it (Figure 1a inset, black). This ionic screening effect is characterized by the Debye screening length λ_D

$$\lambda_D = \sqrt{\frac{\varepsilon k_B T}{q^2 c}} \quad (1)$$

where ε is the dielectric permittivity of the media, k_B is Boltzmann's constant, T is the temperature, q is the electron charge, and c is the ionic strength of the electrolyte solution. For a typical 100 mM buffer solution, λ_D is around 1 nm and the surface potential will be completely screened at a distance of a few nanometers. As the result, most of existing nanoelectronic sensors based on SWNTs or NWs operate either in dry state[9] or in low ionic strength solutions[5,7,12−14,18] (c ~1 nM to 10 mM); otherwise sample will need to undergo a desalting process.[5] Since physiologically relevant ionic strength is ~100 mM, mitigating ionic screening effect is critical for Point-of-Care (POC) nanoelectronic biosensors where detection needs to be carried out at patient site with limited sample processing capability.

In this work, we demonstrate a new high-frequency nanoelectronic sensing platform to overcome the ionic screening effect by operating a SWNT sensor at megahertz frequency range. Our work differs from the conventional techniques of (a) charge based detection,[5−7,9,12,13,15] because we detect biomolecular dipoles at high frequency rather than the associated charges, and (b) impedance spectroscopy,[19,20] because the high transconductance of SWNT FET provides an internal gain for the sensing signal, which obviates the need of external amplification as in case of high-frequency impedance measurement. Further, the frequency mixing due to the nonlinear $I-V$ characteristics of a nanotube FET allows us to operate the sensor at frequencies high enough to overcome ionic screening and yet detect the frequency mixed signals at lower frequencies.

Received: October 18, 2011
Revised: December 1, 2011

   dx.doi.org/10.1021/nl203666a | *Nano Lett.* XXXX, XXX, XXX−XXX

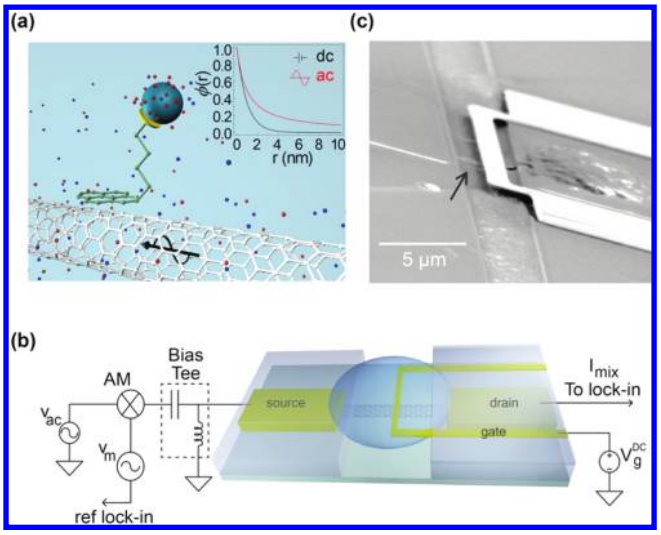

Figure 1. High-frequency SWNT FET sensor and measurement scheme. (a) Schematic of a noncovalently functionalized carbon nanotube in solution. Inset shows the nanotube surface potential induced by a charge at a distance r in dc field (exponential decay, $\phi = \phi_0 e^{-r/\lambda}$) and ac field (flipping dipole, $\phi = \phi_0 \lambda/(r + \lambda)$). (b) Mixing current measurement setup with AM modulated input at source electrode. (c) Scanning electron microscopy image of SWNT FET sensor with a local suspended gate. Channel width ~4 μm.

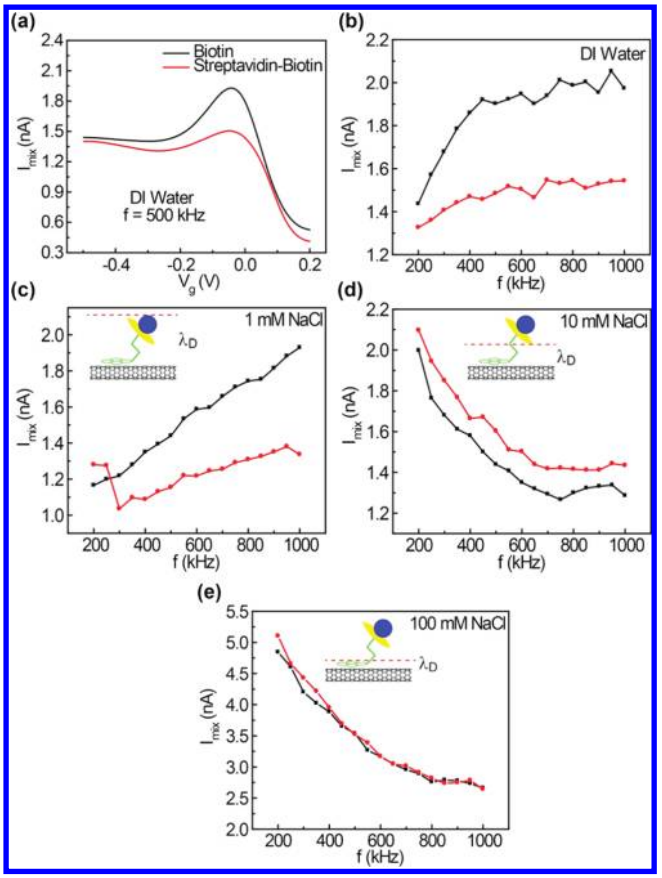

Figure 2. Ionic screening effect observed at dc and low-frequency sensing. (a) I_{mix}–V_g for biotinylated SWNT sensor (black) and streptavidin–biotin bound SWNT sensor (red) in DI water at 500 kHz. Peak values of I_{mix} are plotted over frequencies range of 200 kHz to 1 MHz for biotinylated SWNT (black) and streptavidin–biotin bound SWNT (red) in (b) DI water, (c) 1 mM NaCl, (d) 10 mM NaCl, and (e) 100 mM NaCl as background solutions. Insets in panel c–e illustrate Debye length in each case compared to the biomolecule separation from the sensor surface.

Figure 1a illustrates a model of a biomolecule functionalized SWNT FET sensor excited with an alternating current (ac) field in solution. At dc or low frequency, ions in solution can migrate following the electric field and form the EDL to provide adequate screening. However, at high enough frequencies the ac driving force can no longer overcome the solution drag and the ions in solution do not have sufficient time to form the EDL.[21,22] The surface potential falls off as the inverse of distance instead of exponentially (Figure 1a inset, red). Once the EDL is broken or weakened, the fluctuating dipoles of the target molecule under ac excitation can influence the surface potential of the nanotube, providing a new sensing mechanism.

Figure 1b shows the schematic of our high-frequency SWNT biosensor. SWNT FETs with a suspended top gate electrode structure are fabricated on a $Si_3N_4/SiO_2/Si$ substrate. Single-walled carbon nanotubes were grown by Fe nanoparticle catalyzed chemical vapor deposition.[23,24] Ti/Au (0.5 nm/50 nm) was deposited as the source and drain contact metals. After a blanket deposition of 500 nm SiO_2, the gate electrode was formed by evaporating Cr/Au (50 nm/50 nm). The devices were then covered with 20 nm SiO_2 layer for electrode passivation. The channel (~4 μm wide, Figure 1c) was opened up in the last step with a 1:20 BHF wet etching for nanotube sidewall functionalization. To avoid collapse or buckling of gate electrode,[25] the feature size of suspended part of gate electrode was kept at 25 μm × 1 μm × 100 nm (length × width × thickness). Suspended gate structure was confirmed by SEM imaging (Figure 1c) and the absence of any leakage current between gate and drain contacts.

We configure the SWNT FET as frequency mixer[26,27] wherein its nonlinear current–gate voltage (I–V_g) response mixes high-frequency inputs at the source and gate to yield a mixing current output, I_{mix}, at a lower frequency (Supporting Information Figure S1). We follow the one-source mixing scheme.[28] A high-frequency signal (v_{ac} = 20 mV) is AM modulated by a reference signal (1 V_{p-p}, 1.43 kHz) and fed to the nanotube transistor at the source. The mixing current, I_{mix} is detected at the modulated frequency using a lock-in amplifier. In a typical sensing measurement, ac voltage applied at the source excites oscillating dipoles of the surface-bound biomolecules; the biomolecules thus act as local gate and generate mixing current. Furthermore, the mixing current is directly proportional to the transconductance of the nanotube FET, providing mechanism for in situ signal amplification. Maximum sensitivity thus can be achieved by operating the device at peak transconductance through adjusting the gate voltages.

We choose the biotin–streptavidin ligand–receptor system to evaluate the sensing capability of our high-frequency nanotube sensor in different background ionic strengths. For the surface functionalization of carbon nanotube, we follow the noncovalent scheme provided by Chen et al[29] to preserve the pristine electronic property of nanotubes. The success of nanotube surface functionalization is further confirmed by the shifts in I–V_g transfer curves, and the change in nanotube surface charge density before and after streptavidin binding is estimated to be −3 e/μm (Supporting Information Figure S2).

We first studied the nanotube sensor response in different background ionic strength solutions at relatively lower

dx.doi.org/10.1021/nl203666a | Nano Lett. XXXX, XXX, XXX–XXX

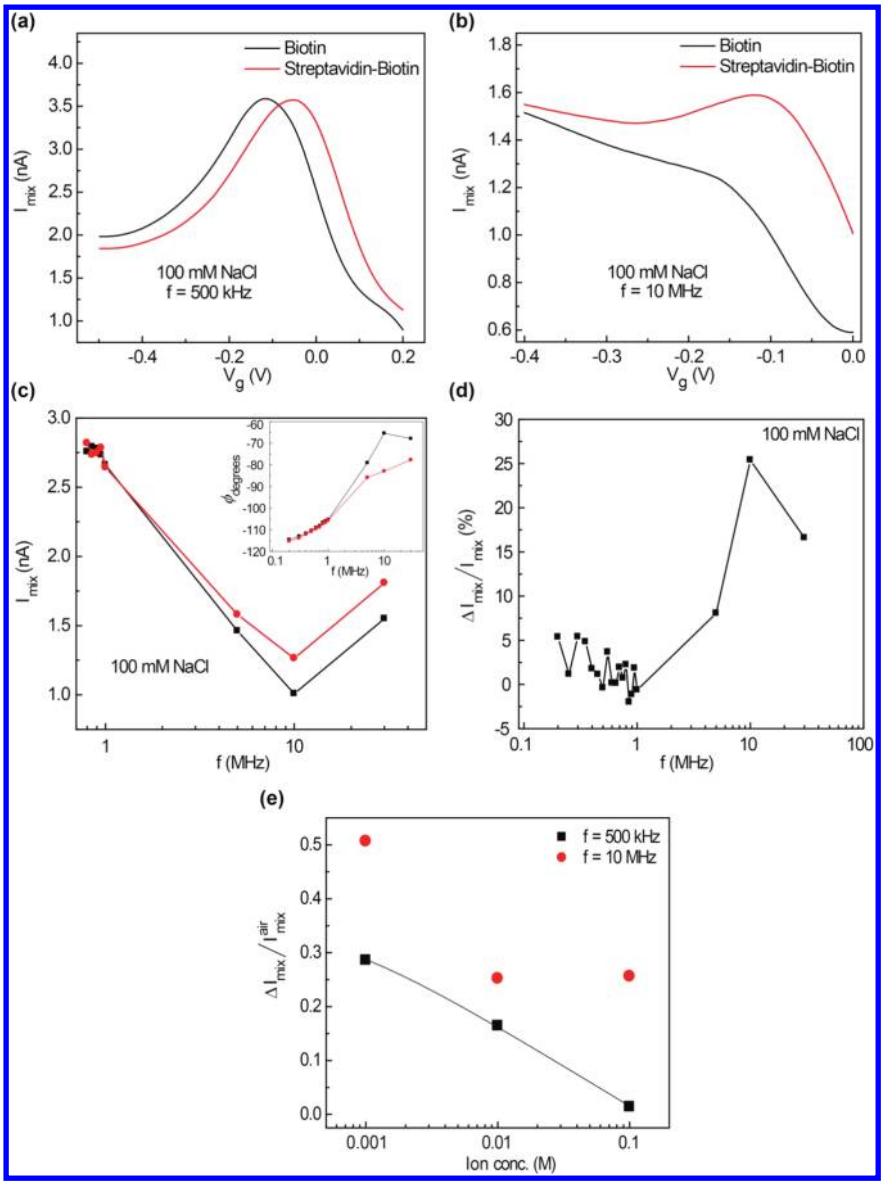

Figure 3. High-frequency sensing mitigates the ionic screening effect and recovers the sensor sensitivity. I_{mix}–V_g curves for biotinylated (black) and streptavidin–biotin bound (red) SWNT in 100 mM NaCl at (a) f = 500 kHz (peak at V_g = −0.117 and −0.053 V, respectively) and (b) f = 10 MHz (peak at V_g = −0.186 V and −0.122 V, respectively). (c) The peak values of I_{mix} are plotted from 800 kHz to 30 MHz for both before (black) and after streptavidin binding (red) in 100 mM NaCl. (Inset) Frequency dependent phase information of I_{mix}. (d) Relative sensitivity, $\Delta I_{mix}/I_{mix}$ of high-frequency SWNT sensor (in percentage) as a function of f. (e) Sensor response with varying background ionic strength at f = 500 kHz (black-filled square) and f = 10 MHz (red-filled circle). The solid line is the logarithmic fit to the experimental data at f = 500 kHz.

frequencies, f (200 kHz to 1 MHz). Figure 2a shows a comparison of I_{mix}–V_g characteristics for the device in DI water at f = 500 kHz. A large difference in I_{mix} was revealed before and after streptavidin binding with mixing current peak at V_g = −0.044 and −0.049 V, respectively. The frequency dependence (200 kHz to 1 MHz) of the peak mixing current are also presented in Figure 2b, and substantial changes in I_{mix} before and after streptavidin binding were observed in DI water. As we increased the background NaCl concentration to 1 mM (Figure 2c) and 10 mM (Figure 2d), differences in I_{mix} before and after streptavidin binding were still visible but smaller than in DI water. Interestingly, when the background salt concentration was increased to 100 mM (Figure 2e), the changes in I_{mix} were no longer visible.

The observed differences of SWNT sensor's low-frequency responses in various background ion concentrations can be explained by the ionic screening effect. The functionalized biomolecules are typically 5–10 nm away from the nanotube surface, which is within or comparable to the Debye lengths in DI water and 1 mM NaCl solution (Figure 2c inset). Hence, under low background ionic strengths, the biomolecule dipoles can still effectively gate the SWNT FET, and the amplified mixing current response can be used to detect the binding event. The changes in the sensing signal become weaker as the buffer concentration is increased by 10 folds to 10 mM NaCl ($\lambda_D \sim 3$ nm). Finally, at 100 mM NaCl concentration, Debye length drops to ~1 nm and no change in mixing current is observed because the dipoles of streptavidin–biotin complex are completely screened away from the nanotube (Figure 2e inset). To confirm that the signal change arises from the binding of streptavidin to the biotinylated device, we also carried out control experiments on fully passivated devices. No

dx.doi.org/10.1021/nl203666a | Nano Lett. XXXX, XXX, XXX–XXX

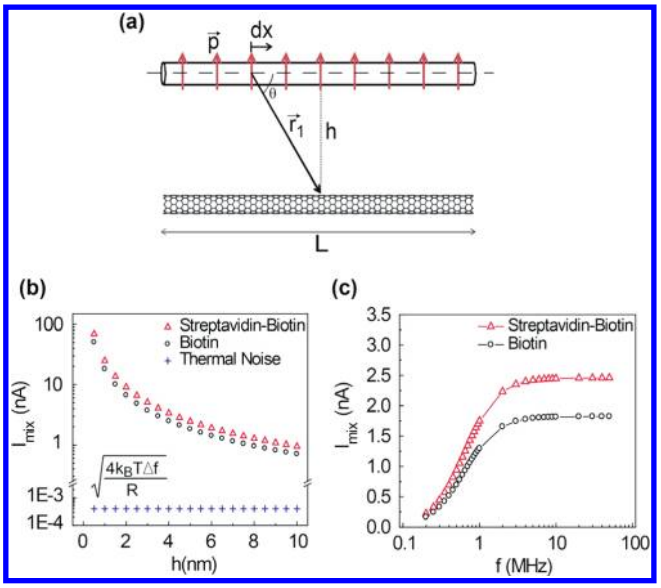

Figure 4. Modeling the high-frequency SWNT FET sensor. (a) One dimensional array of biomolecules with dipole moment, p, above the nanotube surface. (b) Calculated I_{mix} due to a 1D dipole array of biotin (black circle) and streptavidin–biotin complex (red triangle) versus distance from the sensor surface. Thermal noise floor (blue plus sign) is calculated using the device resistance from Supporting Information Figure S2. (c) I_{mix} versus f from our model with biotin and streptavidin–biotin complex separation of h = 5 nm from the sensor surface.

significant mixing current signal change is observed between the two steps even in DI water (Supporting Information Figure S3).

To mitigate the fundamental limit of ionic screening in high ionic strength solution, we operate our SWNT FET sensor at higher frequencies. Figure 3a,b shows the I_{mix}–V_g characteristics of the same device at f = 500 kHz and 10 MHz, respectively, before and after streptavidin binding. At 500 kHz, nanotube sensor cannot differentiate the streptavidin binding. Remarkably however, it recovers its sensitivity when operating at 10 MHz. We also measured the peak values of frequency dependent I_{mix} for the device in 100 mM NaCl solution from 800 kHz to 30 MHz (Figure 3c). Both amplitude and phase signal of I_{mix} suggested nanotube sensor recovered its sensitivity at f > 1 MHz. We further calculated the relative sensitivity, defined as the changes in I_{mix} after streptavidin binding divided by the background I_{mix}, and plotted $\Delta I_{mix}/I_{mix}$ in Figure 3d. Up to 25% change in sensing signal was discovered at f = 10 MHz. In Figure 3e, we plot the change in I_{mix} before and after streptavidin binding with different background ionic concentrations. We observe that at high frequency, the sensor response is enhanced compared to low frequencies and becomes independent of background ionic concentration.

The recovery of the nanotube sensor sensitivity at high frequency can be explained by the breakdown of the charge-screening EDL. At low frequency, the sensor response shows a logarithmic dependence on background ionic concentration (solid line fit in Figure 3e) that has been reported previously in nanowire biosensors.[30] Importantly, when a high-frequency oscillatory signal is applied the salt ions experience a lag due to their finite diffusivity and are unable to follow the excitation field. The first and second adsorbed water layers at the interface undergo molecular relaxation to weaken the EDL capacitor.[22] Therefore, with increasing frequency, the EDL screening decreases and ac electric field penetrates deeper into the solution. This electric field, although attenuated and phase shifted, can now drive the dipoles of the streptavidin–biotin complex. The fluctuating dipoles in turn gate the nanotube to generate a mixing current response greater than the screening limited response at low frequencies (Figure 3e). Typical relaxation time in the double layer estimated[22] to be $10^{-7} \leq \tau_o \leq 10^{-5}$ agrees qualitatively with our observed MHz sensitivity recovery frequency. We also note that the mixing signal drops dramatically at ~30 MHz, which is due to the resonance lost from measurement setup and can be improved in future work.

Last, we calculated the mixing current signal generated from the biomolecules by modeling a 1D array of dipoles located above the nanotube surface as shown in Figure 4a. The molecular dipoles are excited when ac driving voltage is applied onto the nanotube sensor, and the surface bound biomolecules thus act as local gate. The dipole contribution to mixing current can be calculated from (see Supporting Information)

$$I_{mix}^{dipole} = \gamma \frac{m}{2} \frac{\mu C_g'}{L} v_{ac} \phi \cos\theta \qquad (2)$$

where m = 0.78 is the modulation depth for AM signal, μ = 1 $m^2\ V^{-1}\ s^{-1}$ (assuming a nanotube with good device characteristics) is the nanotube carrier mobility, C_g' is the capacitance per unit length between 1D array of dipoles and nanotube, ϕ is the gating potential due to the dipoles, and v_{ac} is the ac drive amplitude. θ denotes the phase lag between the molecular dipoles and the ac drive, and γ represents the attenuation factor (always ≤1) of ac drive amplitude at the molecular dipole site from the nanotube surface. The dipole moment is unable to keep up with the driving field and experiences a frequency dependent phase lag and attenuation because of the EDL screening.[31]

Figure 4b shows the calculated mixing current contributions in a 100 mM ionic background from an array of biotin (dipole moment $\vec{p}$ = 5.4 D[32]) and streptavidin–biotin complex ($\vec{p}$ = 15.72 D[32]) as a function of distance from the sensor surface using eq 2 at high enough frequencies where ionic screening is overcome. At such a condition, attenuation factor γ = 1 and phase lag θ = 0° (see Supporting Information). We observe that as biomolecule moves farther away from the sensor surface, the mixing signal drops roughly as 1/distance (compared to the exponential decay when ionic screening is present). In Figure 4c, we plot the mixing current dependence on frequency taking into account the attenuation and phase factor (eq 2). As the frequency increases, we see a distinguishable change in mixing currents before and after streptavidin binding. At higher frequencies, the weaker double layer leads to smaller phase lag and attenuation and helps recover differences in I_{mix} between the two cases, which agrees with the experimental results in Figure 3c.

On the basis of the theoretical model presented in Figure 4c, we can achieve a relative signal change of 35% for the considered monolayer streptavidin–biotin complex at 5 nm from the sensor surface. In a real operating environment, we also have to deal with the noise fluctuations in the device response. From our device characteristics, we find the thermal noise floor to be ~0.4 pA (Figure 4b); the $1/f$ noise is also negligible at our probing frequencies. Hence, our high-frequency sensing technique is capable of detecting the binding

dx.doi.org/10.1021/nl203666a | Nano Lett. XXXX, XXX, XXX–XXX

of monolayer biomolecules onto sensor surface even in 100 mM ionic strength solution.

The sensitivity of the high-frequency SWNT FET sensor can be further improved by device optimization. From eq 2, I_{mix} depends on dipole gating potential ϕ and device transconductance $\partial G/\partial V_g$. ϕ can be increased by choosing shorter linker molecules and by increasing the receptor coverage to increase the dipole density. The transistor gain can be enhanced by choosing SWNTs with better device characteristics. The high transconductance of the SWNT FET indeed provides an intrinsic gain to amplify the measured high-frequency response. In addition, graphene-based nanoelectronics[33] also have the potential to provide a unique 2D high-frequency biosensor platform. Our results confirm the successful mitigation of fundamental ionic screening effect, which has been hindering the direct adoption of nanoelectronic biosensors in physiologically relevant conditions, and hint a new platform technology for POC biosensing.

■ ASSOCIATED CONTENT

Supporting Information

Mixing current measurement, nanotube sidewall functionalization, modeling, and estimation of mixing current from 1D array of biomolecules. This material is available free of charge via the Internet at http://pubs.acs.org.

■ AUTHOR INFORMATION

Corresponding Author

*E-mail: zzhong@umich.edu.

■ ACKNOWLEDGMENTS

We thank Professor Paul McEuen at Cornell University for early discussion. The work is supported by the start-up fund provided by the University of Michigan. This work used the Lurie Nanofabrication Facility at the University of Michigan, a member of the National Nanotechnology Infrastructure Network funded by the National Science Foundation.

■ REFERENCES

(1) Dekker, C. *Phys. Today* **1999**, *52*, 22−28.
(2) McEuen, P. L.; Fuhrer, M. S.; Park, H. K. *IEEE Trans. Nanotechnol.* **2002**, *1*, 78−85.
(3) Duan, X. F.; Huang, Y.; Cui, Y.; Wang, J. F.; Lieber, C. M. *Nature* **2001**, *409*, 66−69.
(4) Cui, Y.; Zhong, Z. H.; Wang, D. L.; Wang, W. U.; Lieber, C. M. *Nano Lett.* **2003**, *3*, 149−152.
(5) Zheng, G. F.; Patolsky, F.; Cui, Y.; Wang, W. U.; Lieber, C. M. *Nat. Biotechnol.* **2005**, *23*, 1294−1301.
(6) Star, A.; Han, T. R.; Gabriel, J. C. P.; Bradley, K.; Gruner, G. *Nano Lett.* **2003**, *3*, 1421−1423.
(7) Besteman, K.; Lee, J. O.; Wiertz, F. G. M.; Heering, H. A.; Dekker, C. *Nano Lett.* **2003**, *3*, 727−730.
(8) Snow, E. S.; Perkins, F. K.; Houser, E. J.; Badescu, S. C.; Reinecke, T. L. *Science* **2005**, *307*, 1942−1945.
(9) Star, A.; Tu, E.; Niemann, J.; Gabriel, J. C. P.; Joiner, C. S.; Valcke, C. *Proc. Natl. Acad. Sci. U.S.A.* **2006**, *103*, 921−926.
(10) Kong, J.; Franklin, N. R.; Zhou, C. W.; Chapline, M. G.; Peng, S.; Cho, K. J.; Dai, H. J. *Science* **2000**, *287*, 622−625.
(11) McAlpine, M. C.; Ahmad, H.; Wang, D. W.; Heath, J. R. *Nat. Mater.* **2007**, *6*, 379−384.
(12) Heller, I.; Janssens, A. M.; Mannik, J.; Minot, E. D.; Lemay, S. G.; Dekker, C. *Nano Lett.* **2008**, *8*, 591−595.
(13) Patolsky, F.; Zheng, G. F.; Lieber, C. M. *Anal. Chem.* **2006**, *78*, 4260−4269.
(14) Stern, E.; Klemic, J. F.; Routenberg, D. A.; Wyrembak, P. N.; Turner-Evans, D. B.; Hamilton, A. D.; LaVan, D. A.; Fahmy, T. M.; Reed, M. A. *Nature* **2007**, *445*, 519−522.
(15) Stern, E.; Wagner, R.; Sigworth, F. J.; Breaker, R.; Fahmy, T. M.; Reed, M. A. *Nano Lett.* **2007**, *7*, 3405−3409.
(16) Zhang, G. J.; Zhang, G.; Chua, J. H.; Chee, R. E.; Wong, E. H.; Agarwal, A.; Buddharaju, K. D.; Singh, N.; Gao, Z. Q.; Balasubramanian, N. *Nano Lett.* **2008**, *8*, 1066−1070.
(17) Sorgenfrei, S.; Chiu, C.; Johnston, M.; Nuckolls, C.; Shepard, K. L. *Nano Lett.* **2011**, *11*, 3739−3743.
(18) Zheng, G.; Gao, X. P. A; Lieber, C. M. *Nano Lett.* **2010**, *10*, 3179−3183.
(19) Katz, E.; Willner, I. *Electroanalysis* **2003**, *15*, 913−947.
(20) K'Owino, I. O.; Sadik, O. A. *Electroanalysis* **2005**, *17*, 2101−2113.
(21) Han, Z. J.; Morrow, R.; Tay, B. K.; McKenzie, D. *Appl. Phys. Lett.* **2009**, *94*, 043118.
(22) Bockris, J. O.; Gileadi, E.; Muller, K. *J. Chem. Phys.* **1966**, *44*, 1445-&.
(23) Kong, J.; Soh, H. T.; Cassell, A. M.; Quate, C. F.; Dai, H. J. *Nature* **1998**, *395*, 878−881.
(24) Wu, C. C.; Liu, C. H.; Zhong, Z. H. *Nano Lett.* **2010**, *10*, 1032−1036.
(25) Liu, G.; Velasco, J.; Bao, W. Z.; Lau, C. N. *Appl. Phys. Lett.* **2008**, *92*, 203103.
(26) Appenzeller, J.; Frank, D. J. *Appl. Phys. Lett.* **2004**, *84*, 1771−1773.
(27) Rosenblatt, S.; Lin, H.; Sazonova, V.; Tiwari, S.; McEuen, P. L. *Appl. Phys. Lett.* **2005**, *87*, 153111.
(28) Sazonova, V. A *Tunable Carbon Nanotube Resonator*; Cornell University: Ithaca, NY, 2006.
(29) Chen, R. J.; Zhang, Y. G.; Wang, D. W.; Dai, H. J. *J. Am. Chem. Soc.* **2001**, *123*, 3838−3839.
(30) Nair, P. R.; Alam, M. A. *Nano Lett.* **2008**, *8*, 1281−1285.
(31) Kang, K.; Dhont, J. K. G. *Soft Matter* **2010**, *6*, 273−286.
(32) DeChancie, J.; Houk, K. N. *J. Am. Chem. Soc.* **2007**, *129*, 5419−5429.
(33) Wu, Y. Q.; Lin, Y. M.; Bol, A. A.; Jenkins, K. A.; Xia, F. N.; Farmer, D. B.; Zhu, Y.; Avouris, P. *Nature* **2011**, *472*, 74−78.